Finite Element Analysis of Ti-6Al-4V Lattice Cubic Scaffolds for Mandibular Bone Implant Applications

Yasya Khalif Perdana Saleh[1,2,3], Rifky Ismail[1,4,*], Jamari Jamari[1], I Nyoman Jujur[2,3], Suryadi Suryadi[2], Rochmad Winarso[5], Tepi Anggara[3]

[1]Department of Mechanical Engineering, Diponegoro University, Semarang, Indonesia

[2]Biocompatible Material, National Research and Innovation Agency, Tangerang Selatan, Indonesia

[3]Department of Mechanical Engineering, Jakarta Global University, Depok, Indonesia

[4]Center for Biomechanics, Biomaterial, Biomechatronics, and Biosignal Processing (CBIOM3S), Diponegoro University, Semarang, Indonesia

[5]Department of Mechanical Engineering, Faculty of Engineering, Muria Kudus University, Kudus, Indonesia

Received 25 November 2024; received in revised form 24 March 2025; accepted 25 March 2025

DOI: https://doi.org/10.46604/aiti.2024.14542

Abstract

This study evaluates the compressive strength of a cubic lattice scaffold made from Titanium alloy (Ti-6Al-4V) for mandibular bone implants. Scaffold designs with pore sizes ranging from 800 μm to 1000 μm were analyzed using finite element analysis under compressive forces of up to 800 N. Pore sizes of 800 μm and 850 μm achieved a safety factor greater than 1.4, indicating their suitability for both dynamic and static loading. Planned production with bound metal deposition, maintaining a density below 35%, emphasizes material efficiency and cost-effectiveness. Results indicate that 800 μm and 850 μm pore sizes offer optimal strength and safety, suggesting effective mandibular implant integration. Further research on cyclic load testing and osseointegration is recommended.

Keywords: Ti-6Al-4V material strength, lattice beam type cubic scaffold, mandibular bone implant, additive manufacturing, compressive strength

1. Introduction

Bone implants are a medical procedure in orthopedic medicine, replacing injured or missing bone parts with specific materials [1]. Currently, the development of bone implants using additive manufacturing processes has become a captivating topic in research. This process enables the creation of complex shapes unattainable by conventional machining techniques. The main advantage of this technology lies in its ability to generate complex and integrated internal structures, allowing designs that better meet the specific anatomical needs of patients.

In bone implant development, consideration must be given to the complex three-dimensional (3D) geometry and highly organized internal architecture of human skeletal tissue, which cannot be replicated by cells maintained in two dimensions. Porous scaffolds are crucial in hard tissue engineering strategies as they provide a 3D framework. Porous structure characteristics, such as porosity, pore size, and pore interconnectivity, significantly impact biological performance and mechanical properties [2-3]. Research has shown that scaffolds with a porous structure can more effectively support bone regeneration, enabling new tissue growth within the scaffold and better nutrient distribution.

* Corresponding author. E-mail address: rifky_ismail@ft.undip.ac.id

The cubic microarchitecture of the scaffold has a better elasticity modulus and compressive strength compared to other microarchitectures at the same porosity [4]. This also indicates a decrease in low elasticity modulus, making it a suitable choice in bone tissue engineering as it meets the recommended pore size and minimum strength required to support bone growth and integration. Meanwhile, the internal pore structure and material distribution directly influence plasticity and stiffness, determining the stress environment of the surrounding bone tissue when implanted in vivo [5].

Additive manufacturing in mandibular scaffolds is considered to have great potential in accelerating the healing of jawbone defects with outcomes that better match the shape of the existing damage. Literature results show that material selection and 3D printing techniques play an important role in determining the biological compatibility and mechanical effectiveness of the scaffold. Several microarchitecture structures, including body-centered cubic (BCC) and triply periodic minimal surface (TPMS), have been found to have optimal mechanical and biological characteristics for mandibular healing, further strengthening the choice of cubic lattice beam structure as a strong candidate in scaffold design for bone implants [6].

The designed scaffold must be easily printable using specific additive manufacturing techniques. One morphology type commonly developed using this method is the lattice beam cubic type scaffold. Various studies have been conducted to understand its mechanical properties and biocompatibility [7-9]. Cubic scaffolds are widely used due to their mechanical stability and ease of fabrication; however, their biological performance remains a concern, as their regular pore structure may limit cell migration and vascularization [10]. Therefore, further research is needed to explore the influence of pore size and low density on structural strength [11].

This study aims to provide a finite element-based numerical analysis to bridge the knowledge gap and serve as a reference for the bound metal deposition (BMD) manufacturing method, which has been less explored in existing literature [12]. One current implant development is the mandibular bone implant (lower jawbone). This implant has been in development since 2016 [6]. Currently, mandibular bone implant development uses Ti-6Al-4V material with additive manufacturing methods, employing various printing techniques [13-14]. This development has progressed with the adoption of additive manufacturing methods, enabling complex geometries and high precision printing that are difficult to achieve with conventional techniques. This capability to print more precise shapes improves implant integration with the patient's natural bone structure and allows adaptation to significant individual variations among patients. This method opens new possibilities for tailoring implant designs specifically to patient anatomical needs, thus increasing success rates and user comfort. However, further research is needed to understand the complex interactions between scaffold design variables, such as porosity and structural orientation, and the mechanical strength of the resulting scaffold.

Over time, additive manufacturing printing methods have developed, including the use of BMD. This method is a 3D metal printing process based on extrusion, where components are created by depositing metal powder bound with polymer binders [15]. This method can reduce production costs by 60-80% compared to the selective laser sintering (SLS) and electron beam melting (EBM) processes [16]. Global researchers using the BMD method have extensively studied mechanical testing, material characterization, and environmental impacts [15-19]. However, previous studies have primarily focused on print orientation or evaluating the post-print shape of products without providing an in-depth analysis of scaffold mechanical behavior under forces resembling in vivo conditions.

Desktop Metal, one of the additive manufacturing machines using the BMD method, achieves a maximum density of 35% per print. This raises further questions about whether Ti-6Al-4V material with a density below 35% can withstand the forces encountered when applied to mandibular implants. The mandibular bone experiences about 100 N during chewing, with a maximum acceptable force of up to 800 N [20-22]. Additionally, scaffold pore size significantly affects implant mechanical strength. Previous research shows that larger pore sizes reduce the compressive strength of a material [23]. This study will focus on evaluating the compressive strength of the lattice beam cubic-type scaffold using finite element analysis (FEA) simulation, with variations in pore structure porosity and applied force, utilizing Ti-6Al-4V material.

Previous studies have shown that various lattice structures, such as BCC, TPMS, and cubic lattice, have the potential to enhance the mechanical characteristics of scaffolds for mandibular implants [24]. However, further research is needed to explore the influence of pore size and low density on structural strength [7]. In addition, the BMD technology offers a more economical alternative compared to conventional methods like SLS and EBM [25]. Nevertheless, studies focusing on finite element simulation as a reference for the BMD method are still very limited. Therefore, this study presents a novelty by developing a finite element-based simulation as a fundamental reference for further research in the development of the BMD method, without directly evaluating the method itself. By providing a numerical analysis based on finite element simulation, this study can fill the gap in understanding the mechanical strength of Ti-6Al-4V lattice scaffolds with variations in pore size and low density, which has the potential to serve as a reference in the development of BMD-based manufacturing techniques.

The goal of this study is to evaluate the compressive strength of a cubic lattice scaffold made from titanium alloy (Ti-6Al-4V) for mandibular bone implant applications. This study analyzes various pore sizes ranging from 800 µm to 1000 µm using FEA to determine the optimal scaffold configuration that balances mechanical strength, material efficiency, and structural safety. Additionally, this study considers the production feasibility using the method, which maintains a density below 35%. Since this density limitation may affect the scaffold's ability to withstand loads, pore size variation analysis is necessary to assess how a low-density structure can still meet the mechanical requirements for mandibular implant applications effectively and safely.

2. Numerical Methods

This study utilizes two software programs to ensure accurate design and analysis. The student version of Creo is used for developing the porous scaffold model, allowing precise control over structural parameters such as pore size and geometry. ANSYS R2 2022 is then employed for FEA to evaluate the mechanical performance of the scaffold under various loading conditions.

2.1. Geometrical Modelling

This study uses compression test specimens following ISO standards (ISO 13314:2011), with dimensions of 7.2 x 7.2 x 7.2 mm. Pore sizes of 800 µm, 850 µm, 900 µm, 950 µm, and 1000 µm were designed using Creo software, as shown in Fig. 1. The selection of the 800-1000 µm pore size is supported by previous research, such as Wang et al. [26], which demonstrated that an 800 µm pore size offers optimal mechanical properties and enhances osteogenesis, thereby justifying its use in scaffold design. In this study, the analysis is further refined by incorporating 50 µm increments within this range (i.e., 800, 850, 900, 950, and 1000 µm) to provide a more detailed understanding of the variations in mechanical strength at each pore size.

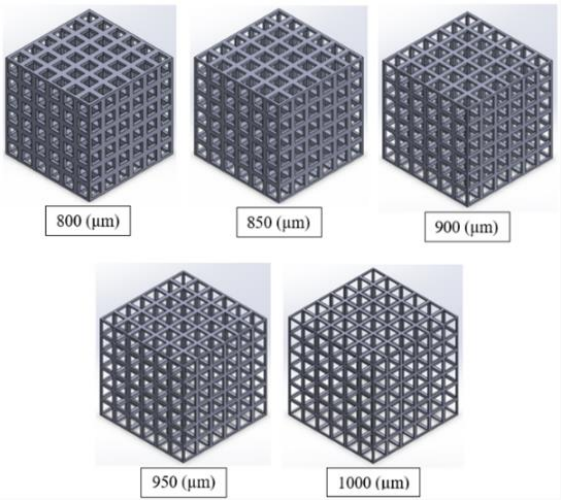

Fig. 1 Cube design with pore variations

Each specified pore size results in a different volume, calculated as follows:

$$V_1 = V_0 - V_h \tag{1}$$

$$V_1 = V_0 - \sum\{Box \times [V_i + (V_o \times 6)]\} \tag{2}$$

where V_1 is the final volume of the porous cube, V_0 is the solid cube volume, V_h is the total hole volume, and $\sum Box$ is the total of all formed hole cells, V_i is the volume of the inner holes, and V_o is the volume of the outer holes, as shown in Fig. 2.

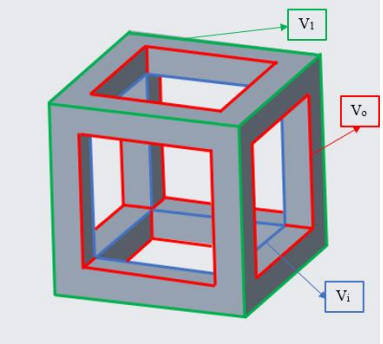

Fig. 2 Cube volume calculation explanation

Differences in pore sizes produce varying infill values for each pore size. The infill can be calculated using Eq. (3):

$$\text{Infill} = \frac{V_1}{V_0} \times 100\% \tag{3}$$

where Infill represents the percentage of the structure's initial volume reduced due to pores (%), V_1 is the final volume of the porous cube, and V_0 is the solid cube volume. Volume and infill values from these calculations are shown in Table 1.

Table 1 Volume and infill values of each pore

No	Pore Size (µm)	Solid Cube Volume (mm^3)	Final Cube Volume (mm^3)	Mass (kg)	Infill (%)
1	800	373.248	96.768	0.00044707	25.92
2	850	373.248	76.734	0.00035451	20.55
3	900	373.248	58.32	0.00026944	15.63
4	950	373.248	41.85	0.00019335	11.21
5	1000	373.248	27.648	0.00012773	7.41

2.2. Material Properties

The compression simulation was performed using ANSYS R2 2022. The first step in operating computational software for FEA is to input the mechanical properties of the material. In this case, the titanium alloy (Ti-6Al-4V) is used as the material for the cubic lattice beam scaffold. Ti-6Al-4V is widely used in biomedical applications due to its high strength-to-weight ratio, corrosion resistance, and excellent biocompatibility.

The mechanical properties are based on Ti-6Al-4V data from Cham et al. [27] research and are included as engineering data available in ANSYS R2 2022, as shown in Table 2. The key properties considered include Young's modulus, Poisson's ratio, tensile strength, yield strength, and density. These properties are essential in ensuring the numerical simulation accurately represents the real-world mechanical behavior of the scaffold. Additionally, the thermal and elastic properties of Ti-6Al-4V were considered, as they influence the material's deformation and load distribution under applied forces.

Table 2 Mechanical properties of titanium alloy or Ti-6Al-4V [27]

No	Property	Value	Unit
1	Density	4620	Kgm^{-3}
2	Coefficient of Thermal Expansion	9.4e-06	C^{-1}
3	Young's Modulus	96000	MPa
4	Poisson's Ratio	0.36	
5	Bulk Modulus	114290	MPa
6	Shear Modulus	35294	MPa
7	Tensile Yield Strength	930	MPa
8	Compressive Yield Strength	930	MPa
9	Tensile Ultimate Strength	1070	MPa

2.3. Mesh Quality Analysis

Mesh analysis focuses on evaluating and optimizing mesh structure to improve accuracy and efficiency in numerical simulations. The quality of the mesh plays a crucial role in determining the reliability of FEA results, as an inappropriate mesh can lead to inaccurate stress distributions or excessive computational costs.

The mesh determination method used in this simulation model is convergence testing, which is beneficial for establishing an optimal mesh size for model development, as it can significantly affect output results [28]. This study tests element sizes from 0.8-0.09 mm with an 800 N load on each model, as illustrated in Fig. 3. Convergence testing ensures that further refinement of the mesh does not significantly alter the results, confirming the balance between computational efficiency and accuracy.

This study tests element sizes from 0.8 mm to 0.09 mm with an 800 N load on each model, as illustrated in Fig. 3. The mesh quality is assessed based on parameters such as skewness, aspect ratio, and Jacobian ratio to ensure high accuracy and numerical stability. Mesh refinement is applied to areas with high stress concentrations to capture critical deformation details while maintaining an efficient computation time.

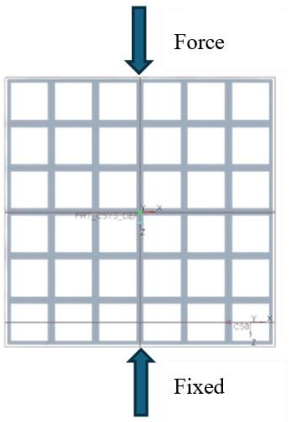

Fig. 3 Force and fixed location

2.4. Force Applied Modelling

After mesh convergence testing, load simulations are conducted based on pore size variations of 800 µm, 850 µm, 900 µm, 950 µm, and 1000 µm, and force variations on each pore size of 100 N, 200 N, 300 N, 400 N, 500 N, 600 N, 700 N, and 800 N. Fig. 4 shows the force application process used in this study's simulations.

The applied forces are based on physiological loading conditions of the mandible (human jawbone), where bite forces typically range from 100 N to 800 N, depending on food texture and biting location. The force is distributed across the scaffold structure to simulate real-world loading conditions. Boundary conditions are applied to simulate constraints, ensuring that movement and deformation occur realistically.

The loading conditions are set to evaluate stress distribution, deformation, and mechanical performance under different forces and pore size variations. This analysis provides insights into how the scaffold withstands physiological forces and ensures its structural integrity under in vivo conditions.

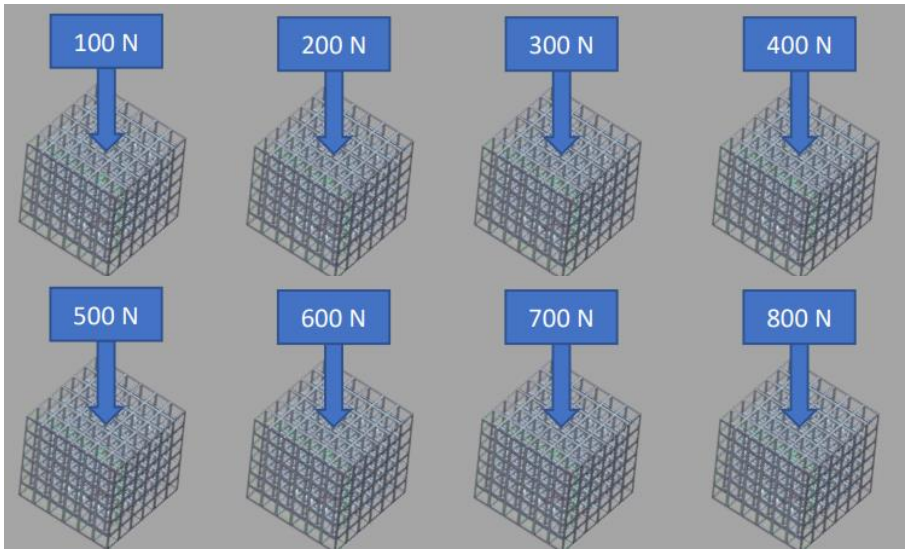

Fig. 4 Force variation in each model

3. Finite Element Analysis

The findings of this study were entirely derived from numerical simulations. These simulations were carefully designed and executed to replicate real-world conditions, ensuring accurate and reliable results. By relying solely on computational methods, the study was able to explore various scenarios and parameters that would be difficult to examine experimentally, thus providing a comprehensive understanding of the phenomena under investigation.

3.1. Results of Mesh Quality Analysis

Using various mesh sizes in the simulation resulted in different node and element counts within the simulation model. The smaller the mesh size, the greater the number of nodes and elements, as the model's geometry is broken down into finer parts. Consequently, a finer mesh requires more complex calculations and more time to complete due to the increased computational load. Fig. 5 shows an example of convergence testing simulation results with an 800 N force and an element size of 0.1 mm.

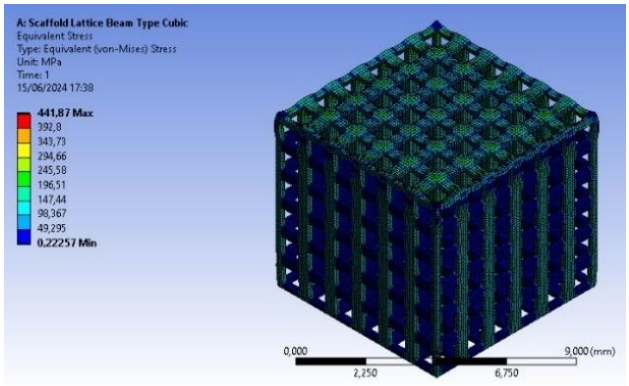

Fig. 5 Sample of simulation results for convergence testing

Based on the data from the convergence test simulation, the Max. von Mises Equivalent Stress value increases inversely with the decrease in element size, as shown in Fig. 6. To quantify the change in Max. von Mises Equivalent Stress, it is necessary to calculate the error value shown in Eq. (4).

$$\text{Error} = \frac{\sigma_1 - \sigma_0}{\sigma_0} \times 100\% \tag{4}$$

Where Error represents the percentage difference in Max. von Mises Equivalent Stress between element sizes (%), σ_0 is the Max. von Mises Equivalent Stress for the smaller element size (MPa), σ_1 is the Max. von Mises Equivalent Stress for the larger element size (MPa). The simulation results indicate that the change in Max. von Mises Equivalent Stress from an element size of 0.8 mm to 0.09 mm is less than 1%, specifically 0.9%, as shown in Table 3.

Table 3 Change in max. von Mises equivalent stress error value

No.	Element Size E_0 (mm)	Max. Stress σ_0 (MPa)	Element Size E_1 (mm)	Max. Stress σ_1 (MPa)	Error (%)
1	0.8	344.61	0.75	351.79	2.08
2	0.75	351.79	0.7	358.97	2.04
3	0.7	358.97	0.65	366.15	1.99
4	0.65	366.15	0.6	373.33	1.96
5	0.6	373.33	0.55	380.50	1.92
6	0.55	380.50	0.5	387.68	1.87
7	0.5	387.68	0.45	394.86	1.85
8	0.45	394.86	0.4	402.04	1.82
9	0.4	402.04	0.35	409.22	1.78
10	0.35	409.22	0.3	416.39	1.75
11	0.3	416.39	0.25	423.57	1.72
12	0.25	423.57	0.2	430.75	1.69
13	0.2	430.75	0.15	437.63	1.67
14	0.15	437.63	0.1	441.87	1.01
15	0.1	441.87	0.09	442.22	0.08

This shows that the change in element size has an insignificant effect, indicating stability in the Maximum von Mises Equivalent Stress value, as illustrated in Fig. 6. The convergence test results confirm that further reduction in element size does not significantly alter the stress distribution, ensuring the reliability of the simulation. A finer mesh may increase computational time without notable improvements in accuracy. Therefore, this study uses an element size of 0.1 mm to achieve a balance between computational efficiency and result accuracy.

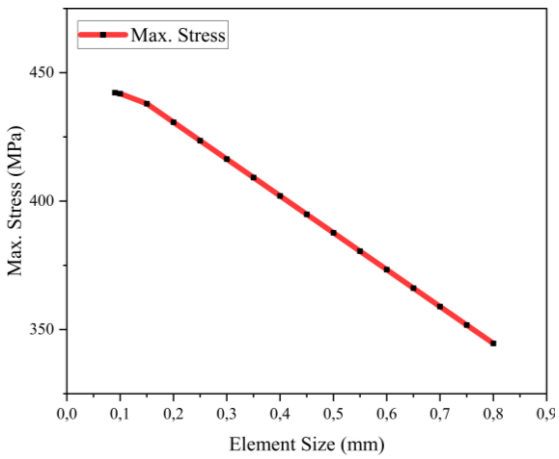

Fig. 6 Convergence test results

3.2. Compression Test Simulation Results Using FEA Software

The compression test in this study was conducted to evaluate the mechanical strength and deformation behavior of Titanium Alloy (Ti-6Al-4V) in a cubic lattice beam scaffold structure. The scaffold was designed with varying pore sizes of 800 µm, 850 µm, 900 µm, 950 µm, and 1000 µm to examine how porosity influences structural integrity under different loading conditions. Applied forces ranged from 100 N to 800 N, simulating physiological loads experienced in mandibular bone applications.

The compression simulation was performed using FEA software to assess the scaffold's mechanical response, including stress distribution, deformation, and failure behavior. The von Mises stress values were recorded to determine the scaffold's ability to withstand compressive loads without exceeding the material's yield strength.

Fig. 7 presents a sample simulation result for the 800 µm pore size under an 800 N force, illustrating the stress concentration and deformation pattern. The results from this analysis provide insight into the optimal pore size and mechanical stability required for mandibular implant applications, ensuring a balance between structural strength and biological compatibility.

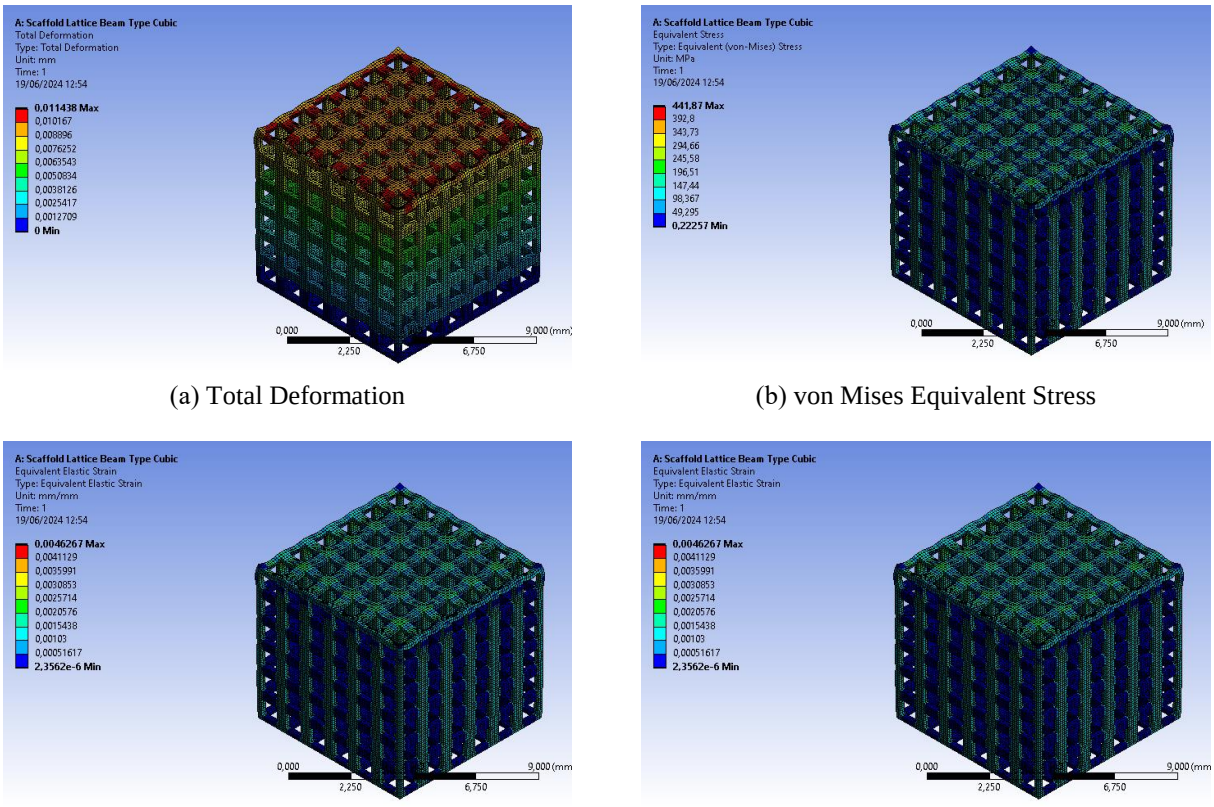

(a) Total Deformation (b) von Mises Equivalent Stress

(c) Equivalent Elastic Strain (d) Safety Factor

Fig. 7 Compression Test Simulation Sample Result Using FEA Software

4. Discussion

The simulation results from the FEA software provided key mechanical parameters, including total deformation, von Mises equivalent stress, equivalent elastic strain, and safety factor. Total deformation analysis helps in understanding the displacement behavior of the scaffold under different loading conditions, ensuring it remains within acceptable limits.

Von Mises equivalent stress was evaluated to determine whether the scaffold could withstand applied forces without exceeding the material's yield strength. Equivalent elastic strain analysis provided insight into the material's ability to deform elastically before reaching plastic deformation.

Additionally, the safety factor was calculated to assess the structural reliability of the scaffold. A higher safety factor indicates a lower risk of failure under physiological loads, ensuring long-term durability and biomechanical compatibility for mandibular bone implant applications.

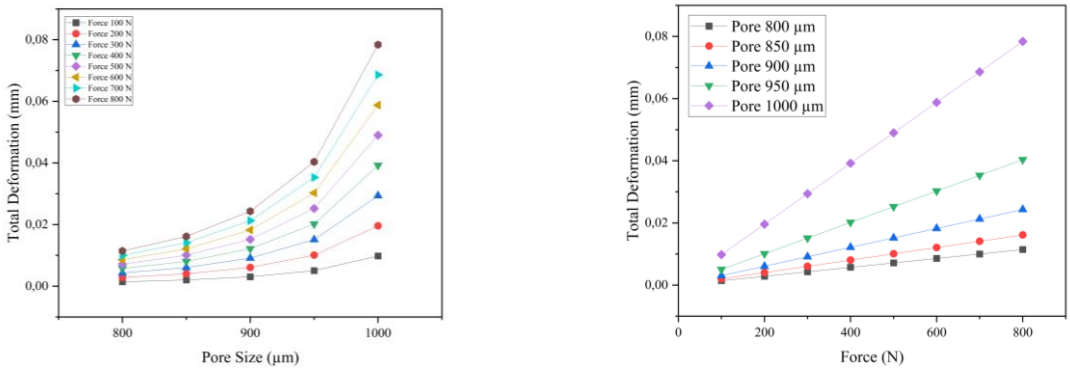

(a) Variation by Force (b) Variation by Pore Size

Fig. 8 Line Graph of Maximum Total Deformation Changes (mm)

The line graph in Fig. 8 indicates that the total deformation value increased with each increment in applied force. Hence, the smaller the applied force, the smaller the resulting shape change, and conversely, the larger the force, the greater the deformation. Additionally, comparing pore size variations reveals that smaller pore sizes correlate with higher material strength, though they also increase material costs. Conversely, larger pore sizes have lower material strength but reduced material costs. When a sufficiently high compressive force is applied to the ductile material, causing deformation beyond its elastic limit, the material enters a plastic deformation phase. This results in a permanent shape change that cannot revert to its original form, unlike elastic deformation, where the material returns to its original shape once the force is removed.

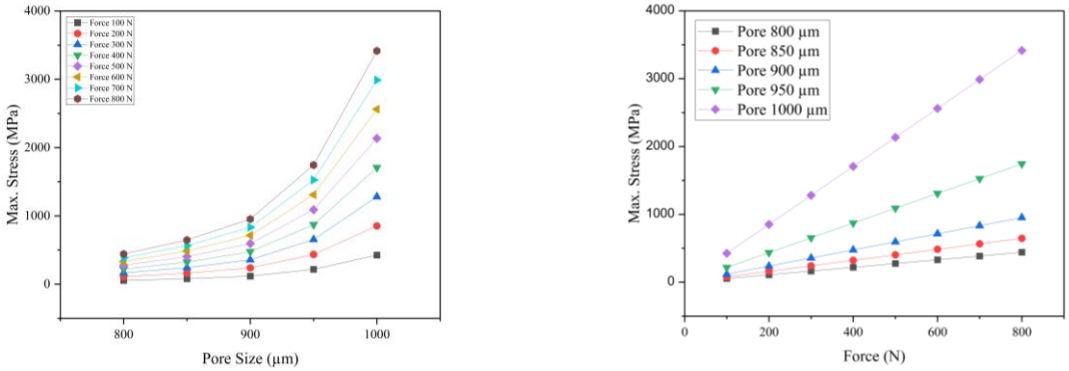

(a) Variation by Force (b) Variation by Pore Size

Fig. 9 Line Graph of Maximum von Mises Equivalent Stress Changes (MPa)

In Fig. 9(a), changes in von Mises Equivalent Stress across different pore sizes under various compressive forces, from 100 N to 800 N, can be observed. The graph shows that von Mises Stress values increase with larger pore sizes and higher applied forces. At the lowest compressive force of 100 N, all pore sizes (800 µm to 1000 µm) exhibited relatively low stress levels, below 500 MPa. However, at 800 N, there was a notable increase in stress, particularly for larger pores such as 950 µm and 1000 µm, where stress values approached or exceeded 3500 MPa. This analysis concludes that larger pores undergo higher stress as compressive force increases. With Ti-6Al-4V's yield strength of 930 MPa, compressive forces up to 400 N are below this limit for all pore sizes (800 µm to 1000 µm), ensuring safety from permanent deformation. However, at 500 N, only pore sizes below 900 µm remain under the yield strength threshold. With higher compressive forces, nearly all pore sizes exceed 930 MPa, except for the 800 µm and 850 µm pores at 800 N, maintaining safe levels at 441.87 MPa and 647.02 MPa, respectively. Therefore, to keep stress below 930 MPa, the optimal pore sizes are 800 µm and 850 µm.

In Fig. 9(b), the von Mises Equivalent Stress is shown by varying the pore sizes (800 µm to 1000 µm) under different forces. The graph results indicate that the larger the pore size, the higher the stress experienced under the same compressive force. For the largest pore size, 1000 µm, even at a low compressive force of 100 N, the von Mises Stress approaches 500 MPa and increases drastically to over 3500 MPa when the compressive force reaches 800 N. Considering the yield strength of 930 MPa, larger pore sizes, such as 1000 µm, tend to deform more rapidly even under lower forces.

Overall, from these two graphs, it can be concluded that to keep the von Mises Equivalent Stress below 930 MPa, a careful combination of pore size and compressive force is necessary. Smaller pore sizes, especially those below 900 µm, can withstand higher forces up to 800 N without exceeding the yield strength. However, for larger pore sizes, particularly those above 850 µm, only lower compressive forces, below 300 N, can be sustained without leading to permanent deformation.

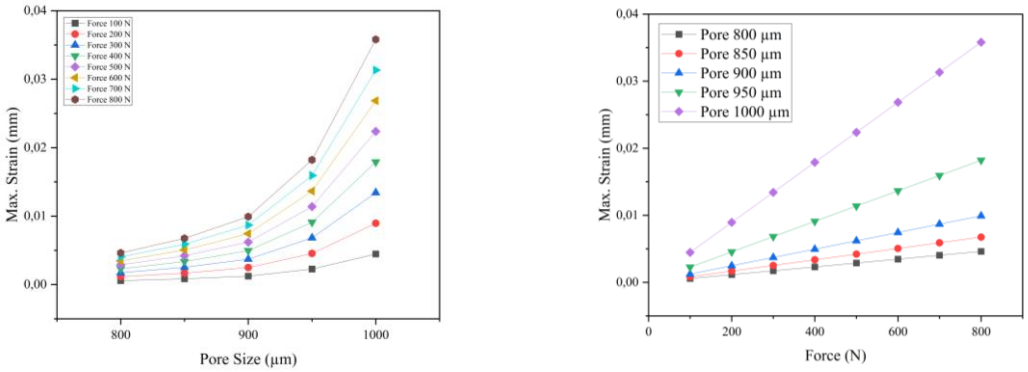

(a) Variation by Force (b) Variation by Pore Size

Fig. 10 Line Graph of Maximum Equivalent Elastic Strain Changes (mm)

Fig. 10 shows that Equivalent Elastic Strain increases with higher compressive force and pore size on the scaffold. In Fig. 10(a), strain variation is shown across forces ranging from 100 N to 800 N, with pore sizes between 800 µm and 1000 µm. Strain values remain relatively low and stable at lower forces. However, they increase significantly at 800 N, especially for larger pore sizes, such as 950 µm and 1000 µm. On the other hand, Fig. 10(b) represents strain across constant compressive forces with varying pore sizes, displays a similar pattern—larger pore sizes yield higher strain values for the same compressive force, peaking around 0.035 mm for a 1000 µm pore size under 800 N. It can be concluded that larger pore sizes tend to produce higher strain under the same compressive force. Therefore, smaller pore sizes, specifically those ranging from 800 µm to 850 µm, are recommended for maintaining mechanical stability in implants.

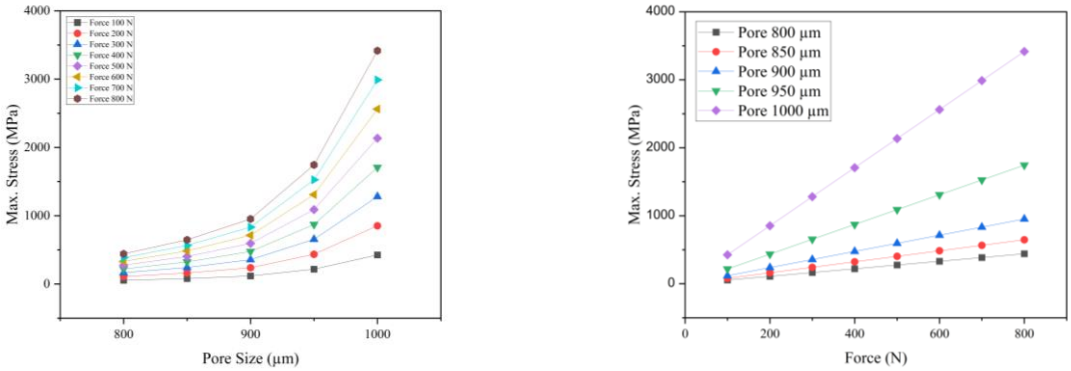

(a) Variation by Force (b) Variation by Pore Size

Fig. 11 Line Graph of Minimum Safety Factor Changes

From Fig. 11, differences in the decline in safety factor values can be observed, influenced by force and pore size variation. Fig. 11(a) shows minimum safety factor changes at different pore sizes with varied forces; the safety factor tends to decrease as pore size increases from 800 µm to 1000 µm. For a maximum load of 800 N, only the 800 µm pore size achieves a

safety factor close to 2.1. This indicates that material with an 800 μm pore size is strong enough to endure dynamic loads safely, making it suitable for applications requiring dynamic load tolerance without excessive cost. In contrast, other pore sizes, with safety factors below 2 at 800 N, may be less ideal for dynamic applications due to potential safety risks. Fig. 11(b) illustrates pore size variation against applied force; only the 850 μm and 800 μm pore sizes maintain safety factors close to 1.5 to 2 at 800 N, specifically at 1.43 and 2.1, respectively.

This analysis demonstrates that material with an 850 μm pore size provides sufficient safety to withstand static force, as its safety factor remains within the acceptable range without overprovisioning. In contrast, pore sizes exceeding 850 μm, with safety factors below 1.5, may be less suitable for static applications at 800 N. The 1.5 safety factor threshold is considered based on Shash et al. [29] research on mandibular bone implants established that a minimum safety factor of at least 1.5 is required to ensure structural integrity while avoiding excessive material usage. This threshold provides a balance between mechanical performance and material efficiency, ensuring that the scaffold can withstand physiological loads while remaining cost-effective. If the safety factor is too high, as is often the case with smaller pores under low force, it results in excessive costs due to additional strength that is not required. Hence, to optimize both cost and performance, a pore size of 800 μm at 800 N dynamic load is ideal for dynamic needs, while the 850 μm pore size is more suitable for static needs at the same load, providing a sufficient safety factor without being excessive.

The results of this study align with previous research on lattice scaffold designs for mandibular implants. Studies such as Liu et al. [30] have investigated various lattice structures, including simple cubic, BCC, and side centered cubic, and reported comparable trends in mechanical performance. However, variations in pore size, porosity, and unit cell geometry may influence the overall scaffold performance, highlighting the need for further comparative analysis. Compared to the study by Wang et al. [26], which found that pore sizes of 900 μm and 1000 μm are more favorable for promoting osteoblast proliferation and differentiation, their mechanical strength is insufficient to withstand the maximum load on a mandibular bone implant. Although larger pore sizes (900 μm to 1000 μm) enhance bone regeneration, their structural integrity might not be adequate for supporting functional loads. Therefore, to complement the conclusions of Wang et al. [26], pore sizes of 800 μm and 850 μm can be considered an optimal solution for determining scaffold pore size in mandibular bone implants, as they offer a balance between mechanical stability and potential for osteointegration.

5. Conclusions

This study successfully analyzed the mechanical strength of Titanium Alloy / Ti-6Al-4V in a cubic lattice beam scaffold structure with pore sizes ranging from 800 μm to 1000 μm under various compressive forces using FEA software. The findings emphasize the influence of pore size on the structural performance and suitability of the scaffold for mandibular bone implant applications. Key conclusions are summarized as follows:

(1) Scaffolds with pore sizes of 800 μm and 850 μm exhibit safety factors and von Mises equivalent stresses within acceptable limits for compressive forces up to 800 N, ensuring structural safety and integrity.
(2) At 800 N, the 800 μm pore size achieves a safety factor of 2.1, making it suitable for dynamic loads, while the 850 μm pore size with a safety factor of 1.43 is more appropriate for static loads.
(3) Despite having densities below 35%, the scaffold structure demonstrates excellent material utilization and production cost efficiency. The densities for 800 μm and 850 μm pore sizes are 25.92% and 20.55%, respectively, meeting mechanical strength requirements for mandibular bone implants.
(4) The BMD printing method effectively produces scaffolds with safe and strong structures, highlighting the method's potential for cost-effective and material-efficient orthopedic implant development.

Future studies should focus on further investigating the impact of pore size on scaffold performance and suitability. Suggested areas for improvement and focus include:

(1) To improve reliability and applicability, cyclic load testing on physical samples is essential to evaluate the scaffold's resistance to repetitive forces, such as chewing.
(2) Further biocompatibility testing and analysis of porosity effects on bone growth are necessary to ensure optimal implant integration and long-term safety for patients.

These results contribute to advancing titanium bone implant technology, providing a pathway to more effective, durable, and affordable solutions in orthopedic medicine.

Conflicts of Interest

The authors declare no conflict of interest.

References

[1] "BRIN Kembangkan Riset Material untuk Implan Tulang," https://www.brin.go.id/news/110583/brin-kembangkan-riset-material-untuk-implan-tulang, accessed in 2024.
[2] C. Shuai, et al., "An nMgO Containing Scaffold: Antibacterial Activity, Degradation Properties and Cell Responses," International Journal of Bioprinting, vol. 4, no. 1, article no. 120, 2018.
[3] J. He, F. Xu, R. Dong, B. Guo, and D. Li, "Electrohydrodynamic 3D Printing of Microscale Poly (ε-Caprolactone) Scaffolds with Multi-Walled Carbon Nanotubes," Biofabrication, vol. 9, no. 1, article no. 015007, 2017.
[4] R. Winarso, R. Ismail, P. W. Anggoro, J. Jamari, and A. P. Bayuseno, "Numerical Study on Mechanical Properties of Cubic Porous Bone Scaffold: Effect of Unit Cell Type," AIP Conference Proceedings, vol. 3074, no. 1, article no. 020001, 2024.
[5] M. Guvendiren, J. Molde, R. M. D. Soares, and J. Kohn, "Designing Biomaterials for 3D Printing," ACS Biomaterials Science & Engineering, vol. 2, no. 10, pp. 1679-1693, 2016.
[6] R. Winarso, R. Ismail, P. W. Anggoro, J. Jamari, and A. P. Bayuseno, "A Scoping Review of the Additive Manufacturing of Mandibular Implants," Frontiers in Mechanical Engineering, vol. 9, article no. 1079887, 2023.
[7] S. Dhiman, et al., "Cubic Lattice Structures of Ti6Al4V under Compressive Loading: Towards Assessing the Performance for Hard Tissue Implants Alternative," Materials, vol. 14, no. 14, article no. 3866, 2021.
[8] R. Winarso, R. Ismail, P. W. Anggoro, J. Jamari, and A. P. Bayuseno, "Finite Element Analysis of Irregular Porous Scaffold for Bone Tissue Engineering," ARPN Journal of Engineering and Applied Sciences, vol. 18, no. 6, pp. 569-580, 2023.
[9] R. Winarso, P. W. Anggoro, R. Ismail, J. Jamari, and A. P. Bayuseno, "Application of Fused Deposition Modeling (FDM) on Bone Scaffold Manufacturing Process: A Review," Heliyon, vol. 8, no. 11, article no. e11701, 2022.
[10] C. Ghayor, T. H. Chen, I. Bhattacharya, M. Ozcan, and F. E. Weber, "Microporosities in 3D-Printed Tricalcium-Phosphate-Based Bone Substitutes Enhance Osteoconduction and Affect Osteoclastic Resorption," International Journal of Molecular Sciences, vol. 21, no. 23, article no. 9270, 2020.
[11] C. Ghayor and F. E. Weber, "Osteoconductive Microarchitecture of Bone Substitutes for Bone Regeneration Revisited," Frontiers in Physiology, vol. 9, article no. 960, 2018.
[12] S. Rasheed, W. Lughmani, M. A. Obeidi, D. Brabazon, and I. Ahad, "Additive Manufacturing of Bone Scaffolds Using PolyJet and Stereolithography Techniques," Applied Sciences, vol. 11, no. 16, article no. 7336, 2021.
[13] A. Dutta, K. Mukherjee, S. Dhara, and S. Gupta, "Design of Porous Titanium Scaffold for Complete Mandibular Reconstruction: The Influence of Pore Architecture Parameters," Computers in Biology and Medicine, vol. 108, pp. 31-41, 2019.
[14] W. M. Peng, et al., "Biomechanical and Mechanostat Analysis of a Titanium Layered Porous Implant for Mandibular Reconstruction: The Effect of the Topology Optimization Design," Materials Science and Engineering: C, vol. 124, article no. 112056, 2021.
[15] I. Bianchi, V. Di Pompeo, T. Mancia, M. Pieralisi, and A. Vita, "Environmental Impacts Assessment of Bound Metal Deposition 3D Printing Process for Stainless Steel," Procedia CIRP, vol. 105, pp. 386-391, 2022.

[16] A. Watson, J. Belding, and B. D. Ellis, "Characterization of 17-4 PH Processed via Bound Metal Deposition (BMD)," Proceedings of TMS 2020 149th Annual Meeting & Exhibition Supplemental Proceedings, Springer, Cham, pp. 205-216, 2020.

[17] D. G. Luchinsky, et al., "Multi-Scale Modelling of the Bound Metal Deposition Manufacturing of Ti6Al4V," Thermo, vol. 2, no. 3, pp. 116-148, 2022.

[18] V. Di Pompeo, et al., "Microstructure and Defect Analysis of 17-4PH Stainless Steel Fabricated by the Bound Metal Deposition Additive Manufacturing Technology," Crystals, vol. 13, no. 9, article no. 1312, 2023.

[19] F. Bjørheim and I. M. La Torraca Lopez, "Tension Testing of Additively Manufactured Specimens of 17-4 PH Processed by Bound Metal Deposition," IOP Conference Series: Materials Science and Engineering, vol. 1201, no. 1, article no. 012037, 2021.

[20] S. N. Huang, et al., "Biomechanical Assessment of Design Parameters on a Self-Developed 3D-Printed Titanium-Alloy Reconstruction/Prosthetic Implant for Mandibular Segmental Osteotomy Defect," Metals, vol. 9, no. 5, article no. 597, 2019.

[21] C. H. Li, C. H. Wu, and C. L. Lin, "Design of a Patient-Specific Mandible Reconstruction Implant with Dental Prosthesis for Metal 3D Printing Using Integrated Weighted Topology Optimization and Finite Element Analysis," Journal of the Mechanical Behavior of Biomedical Materials, vol. 105, article no. 103700, 2020.

[22] C. L. Lin, Y. T. Wang, C. M. Chang, C. H. Wu, and W. H. Tsai, "Design Criteria for Patient-Specific Mandibular Continuity Defect Reconstructed Implant with Lightweight Structure Using Weighted Topology Optimization and Validated with Biomechanical Fatigue Testing," International Journal of Bioprinting, vol. 8, no. 1, article no. 437, 2021.

[23] Z. Chen, et al., "Influence of the Pore Size and Porosity of Selective Laser Melted Ti6Al4V ELI Porous Scaffold on Cell Proliferation, Osteogenesis and Bone Ingrowth," Materials Science and Engineering. C, Materials for Biological Applications, vol. 106, article no. 110289, 2020.

[24] R. Alkentar, F. Mate, and T. Mankovits, "Investigation of the Performance of Ti6Al4V Lattice Structures Designed for Biomedical Implants Using the Finite Element Method," Materials (Basel, Switzerland), vol. 15, no.18, article no. 6335, 2022.

[25] X. Xu, D. Luo, C. Guo, and Q. Rong, "A Custom-Made Temporomandibular Joint Prosthesis for Fabrication by Selective Laser Melting: Finite Element Analysis," Medical Engineering & Physics, vol. 46, pp. 1-11, 2017.

[26] C. Wang, et al., "Effect of Pore Size on the Physicochemical Properties and Osteogenesis of Ti6Al4V Porous Scaffolds with Bionic Structure," ACS Omega, vol. 5, no. 44, pp. 28684-28692, 2020.

[27] Y. R. K. Cham, S. S. Hoshi, and S. V. Nimje, "Innovation in the Impact Structure Design of a Four Wheel Automobile," International Research Journal of Engineering and Technology, vol. 5, no. 9, pp. 84-87, 2018.

[28] M. Ahmad, K. A. Ismail, and F. Mat, "Convergence of Finite Element Model for Crushing of a Conical Thin-Walled Tube," Procedia Engineering, vol. 53, pp. 586-593, 2013.

[29] Y. H. Shash, M. T. El-Wakad, M. A. A. Eldosoky, and M. M. Dohiem, "Evaluation of Stress and Strain on Mandible Caused Using “All-on-Four” System from PEEK in Hybrid Prosthesis: Finite-Element Analysis," Odontology, vol. 111, no. 3, pp. 618-629, 2023.

[30] B. Liu, et al., "The Optimization of Ti Gradient Porous Structure Involves the Finite Element Simulation Analysis," Frontiers in Materials, vol. 8, article no. 642135, 2021.